Role of Low Flow and Backward Flow Zones on Colloid Transport in Pore Structures Derived from Real Porous Media

ARTICLE *in* ENVIRONMENTAL SCIENCE AND TECHNOLOGY · JULY 2010

Impact Factor: 5.33 · DOI: 10.1021/es903647g · Source: PubMed

3 AUTHORS, INCLUDING:

Xiqing Li
Peking University
38 PUBLICATIONS **974** CITATIONS

SEE PROFILE

Dongxiao Zhang
Peking University
181 PUBLICATIONS **3,972** CITATIONS

SEE PROFILE

Environ. Sci. Technol. **2010,** *44,* 1274–1280

Tracking Colloid Transport in Porous Media Using Discrete Flow Fields and Sensitivity of Simulated Colloid Deposition to Space Discretization

ZHELONG LI,[†,‡] DONGXIAO ZHANG,[‡] AND XIQING LI*[,†,‡]

Laboratory of Earth Surface Processes, College of Urban and Environmental Sciences and Department of Energy and Resources Engineering, College of Engineering, Peking University, Beijing, 100871, P. R. China

Received September 14, 2009. Revised manuscript received November 23, 2009. Accepted January 5, 2010.

Advances in pore structure characterization and lattice−Boltzmann (LB) simulations of flow fields in pore spaces are making mechanistic simulations of colloid transport in real porous media a realistic goal. The primary challenge to reach this goal may be the computational demand of LB flow simulations in discretized porous medium domains at an assemblage scale. In this work, flow fields in simple cubic and dense packing systems were simulated at different discretization resolutions using the LB method. The simulated flow fields were incorporated into to a three-dimensional particle tracking model to simulate colloid transport in the two systems. The simulated colloid deposition tended to become asymptotic at a critical discretization resolution (voxel−grain size ratio = 0.01) at groundwater flow regimes for colloids down to submicrometer level under favorable conditions and down to around 1 μm under unfavorable conditions. The average simulated fluid velocities near grain surfaces were extracted to explain the sensitivities of simulated depositions to space discretization under both conditions. At the critical discretization resolution, current computation capacity would allow flow simulations and particle tracking in assemblage porous medium domains. In addition, particle tracking simulations revealed that colloids may be retained in flow vortices under conditions both favorable and unfavorable for deposition. Colloid retention in flow vortices has been proposed only very recently. Here we provide a mechanistic confirmation to this novel retention process.

Introduction

Predicting the fate and transport of colloids in porous media is of great importance to many engineered and natural processes, such as filtration in water and wastewater treatment, contaminant transport facilitated by colloids, and natural filtration of pathogens in subsurface. To date, the prediction tool most commonly used for colloid transport in saturated porous media has been the classical filtration theory (CFT) (*1*). This theory is based on the so-called sphere-in-cell model that idealizes the porous media as an assemblage of spherical collectors, each surrounded by a spherical shell of fluid (*2*). On the basis of the idealized pore structure, colloid trajectory analysis can be carried out by performing force and torque balances to calculate the probability that colloids will be collected (*3*−*5*).

CFT predicts colloid transport in porous media reasonably well under the so-called favorable deposition conditions where the overall interaction between the grain and colloid surfaces is attractive (e.g., refs *3, 4, 6*). However, dramatic discrepancies between CFT predictions and experimental observations exist under the unfavorable conditions where the overall interaction between the collector grain and colloid surfaces is repulsive and an energy barrier to deposition exists. Under such conditions, CFT predicts that colloid deposition would be negligible at most, whereas numerous laboratory and field studies demonstrated that significant colloid deposition occurs commonly (e.g., ref *7*). The observed discrepancies were traditionally attributed to the neglect of grain and colloid surface charge heterogeneity and roughness in CFT (e.g., refs *8, 9*). Recently, the inability of CFT to account for the complex pore geometries of real porous media has also been recognized as an important factor that contributes to the observed discrepancies. Experimental observations and theoretical simulations both indicate that a significant amount of colloids can be deposited at grain-to-grain contacts and retained in zones of flow stagnation via association with the secondary energy minimum (*10*−*14*). Neither grain-to-grain contacts nor zones of flow stagnation are reflected in CFT.

Explicit incorporation of the complex geometries in real porous media into trajectory analysis was historically impossible due to lack of the technology that could precisely characterize the pore structure. Another hurdle for colloid trajectory analysis in real porous media was the unavailability of accurate flow fields in the complex pore spaces. The lack of flow fields precludes the calculation of the fluid drags that suspended colloids experience, thus disallowing force balances to be performed to track colloid trajectories. Recent advances in X-ray microtomography (XMT) and lattice−Boltzmann (LB) flow simulations, however, are making these hurdles surmountable. XMT can provide an exact 3-D rendering of the pore structure and allows direct observation of colloid deposition in porous media (*10, 11, 15*).

From the XMT-derived pore structure, LB flow simulations can be implemented to calculate the flow field in the pore space (e.g., ref *15*). The LB method considers a typical volume of fluid as a collection of particles that are represented by a distribution function at each grid point in a discretized domain. The time is discretized as well, and the fluid particles can collide with each other as they move according to a set of rules. These rules are designed in such a manner that the governing continuity and the Navier−Stokes equation are recovered. The LB method is powerful in dealing with single and multiphase flow problems in complex geometries (*16*). There have been several studies in the literature that combined LB simulations and pore structure characterization techniques to examine colloid transport in porous media. For example, Chen et al. used XMT and LB simulations to examine the temporal evolution of pore geometries, fluid flow, and solute transport following colloid deposition (*17, 18*), and Creber et al. combined LB simulations with a nuclear magnetic resonance technique to quantify the velocity acceleration factor for colloid transport (*19*).

Although particle tracking implemented at pore scales is useful in elucidating colloid deposition and retention mechanisms (e.g., refs *12, 13*), it must be extended to at least

* Corresponding author phone/fax: 86-10-62753246; e-mail: xli@urban.pku.edu cn.
† Laboratory of Earth Surface Processes.
‡ Department of Energy and Resources Engineering.

10.1021/es9027716

Published on Web 01/20/2010

assemblage scales to achieve minimum representativeness of real porous media required for the simulation to have any predictive meaning. However, applying LB flow simulations to particle tracking in an assemblage-scale porous medium domain (that consists of at least several grains in each dimension) is computationally demanding, as simulating flow in a domain with only 100 × 100 × 100 voxels could easily take tens of hours on a personal computer. The accuracies of simulated flow fields and colloid deposition obviously increase as discretization of pore space gets finer. However, with discretization fine enough to yield an accurate flow field, LB simulations may be prohibitively expensive in computation.

The objective of this work, therefore, was to examine the sensitivity of simulated colloid deposition to discretization of pore spaces and the effects of grain size, colloid size, fluid velocity, and solution chemistry on the sensitivity. LB flow simulations were performed in two packing systems at different discretization resolutions. The simulated flow fields were incorporated into a three-dimensional particle tracking model to simulate colloid transport in the two systems. The ultimate goal was to determine the lowest discretization resolution that would yield accurate simulated colloid deposition. The feasibility of extending particle tracking to assemblage porous medium domains using flow fields at this discretization resolution was discussed. In addition, a potentially new colloid retention process was elucidated.

Methodology

Pore Structures. Particle tracking was performed in unit cells of the simple cubic (SC) and dense packing (DC) systems to examine the sensitivity of simulated colloid deposition to pore space discretization. Both systems contain grain-to-grain contacts that exist in real porous media, as demonstrated by XMT (*10, 12*). The porosities of the simple cubic and dense packing systems are 0.476 and 0.26, respectively, thus bracketing the porosities of porous media commonly encountered in laboratories and fields.

It is convenient to choose unit cells with entry planes at $z = 0$ or $z = 1$ for SC and $z = -1.414$ or $z = 0$ for DC, where the z value is dimensionless as being normalized to the grain radius (Figure S1, Supporting Information). The $x-y$ boundaries of the unit cells were from 0 to 2 for SC and from −1 to 1 for DC, respectively. Particle tracking using approximate analytical solution of flow fields in the two systems indicated no deposition in the unit cell with entry plane at $z = 1$ for SC and roughly equivalent deposition at the two unit cells of DC (*13*). Simulations in this work therefore were performed in only one unit cell for each packing system, the one with entry plane at $z = 1$ for SC and the one with entry plane at $z = -1.414$ for DC. The unit cells of the two packing systems and the associated coordinate systems are shown in the Supporting Information (Figure S1) and in a previous paper (*13*).

LB Simulation of Flow Fields. The unit cells were discretized to different resolutions for LB flow simulations. Voxel (i.e., small cube) lengths of $^1/_{50}$ (0.02), $^1/_{100}$ (0.01), $^1/_{150}$ (0.0067), and $^1/_{200}$ (0.005) of the grain diameter were used for discretization, yielding 50 × 50 × 50, 100 × 100 × 100, 150 × 150 × 150, and 200 × 200 × 200 voxels, respectively, for the SC unit cell. The voxel−grain size ratio at the lowest resolution here is smaller than those used in most previous LB simulation studies. Since the DC unit cell has a greater noninteger length (2.828 as normalized to grain radius) in the z dimension, 50 × 50 × 72, 100 × 100 × 144, 150 × 150 × 216, and 200 × 200 × 288 voxels were used. The simulated space extended out by a small distance from both the inlet and outlet end of the unit cell and had a slightly greater z-direction length of 2.88 (from −1.44 to 1.44). Only the flow field within the unit cell was used for particle tracking.

A D3Q15 lattice−Boltzmann BGK model was used to perform flow simulations in the unit cells. Governing equations of the model are provided in the Supporting Information. The boundary conditions of flow simulations are described as follows. Inside the unit cells, if the distance of a node to any of a grain center is less or greater than the grain radius, the node is assigned a Boolean number of 1 or 0 to represent solid (flow velocity = 0) and fluid, respectively. The solid (no-slip) nodes at the grain surface were applied with the bounce back rule, which means that the unknown populations of the inward-pointing links are assigned the known values of their outward pointing counterparts (*20*). The periodicity of the packing systems allowed the use of periodic boundaries at the bounding x and y planes. This was done by setting the stream function of time step N in a particular direction at one side of the domain equal to the stream function of time step $N - 1$ in the same direction at the opposite side of the domain.

The treatment of pressure (density) boundaries followed that of Zou and He (*21*). A pressure (density) difference ($\Delta\rho = 0.0001$) was applied at the inlet and outlet boundaries ($z = 1$ and 3 for SC and −1.44 and 1.44 for DC) of the simulated spaces. The z-direction velocities at one cross section perpendicular to the z direction were integrated to yield the superficial velocity (v_s) corresponding to the applied density difference (v_s is the same at all cross sections according to fluid continuity). The velocities in the simulated space were divided by v_s to obtain a dimensionless flow field (assuming creeping flow). During particle tracking, the dimensionless velocities were turned dimensional by multiplying the superficial velocity (V) selected for a simulation. Validation of the LB simulation code is presented in the Supporting Information.

Particle Tracking. The colloid trajectories in the pore spaces are tracked by performing force and torque balances to determine the colloid velocities in three dimensions. The force and torque balances and the derivation of colloid velocities are described in detail in a previous publication (*13*), with minor changes provided in the Supporting Information. The forces that affect colloid movement include virtual mass, gravity, electric double layer, van der Waals, Brownian, driving fluid drag, and resisting fluid drag. Colloid−colloid interaction was not considered. The fluid velocities needed to calculate the driving and resisting fluid drag are derived from the flow field simulated using the LB method. Since a flow field calculated by LB simulations is discrete in nature, a trilinear interpolation algorithm was used to obtain fluid velocities at any position in the pore space (Supporting Information).

Simulation Conditions and Protocols. Simulations were conducted at different discretization resolutions using three grain diameters ($d_g = 150, 300, 600\ \mu$m), five colloid diameters ($d_p = 0.5, 1.5, 3.0, 6.0, 12.0\ \mu$m), and three superficial fluid velocities (4.0×10^{-4}, 1.71×10^{-5}, 4.28×10^{-6} m s^{-1}), under both favorable and unfavorable deposition conditions. The favorable conditions were created by assigning a collector ζ-potential of −60 mV and a colloid ζ-potential of +20 mV, whereas the unfavorable conditions were created by assigning negative ζ-potentials for both colloids and collectors (see Supporting Information for details). The range of grain sizes here (150−600 μm) are also typically examined in other laboratory studies or encountered in the field. The highest superficial velocity represents flow regimes in engineered water treatment systems such as rapid filtration. The medium and low velocities correspond to fluid velocities of about 4.0 and 1.0 m d^{-1} (at a typical porosity of 0.36), respectively, reflecting groundwater flow conditions.

Under each simulation condition, four simulation runs using four different random seeds (the number used to generate particle entry positions) were performed to allow

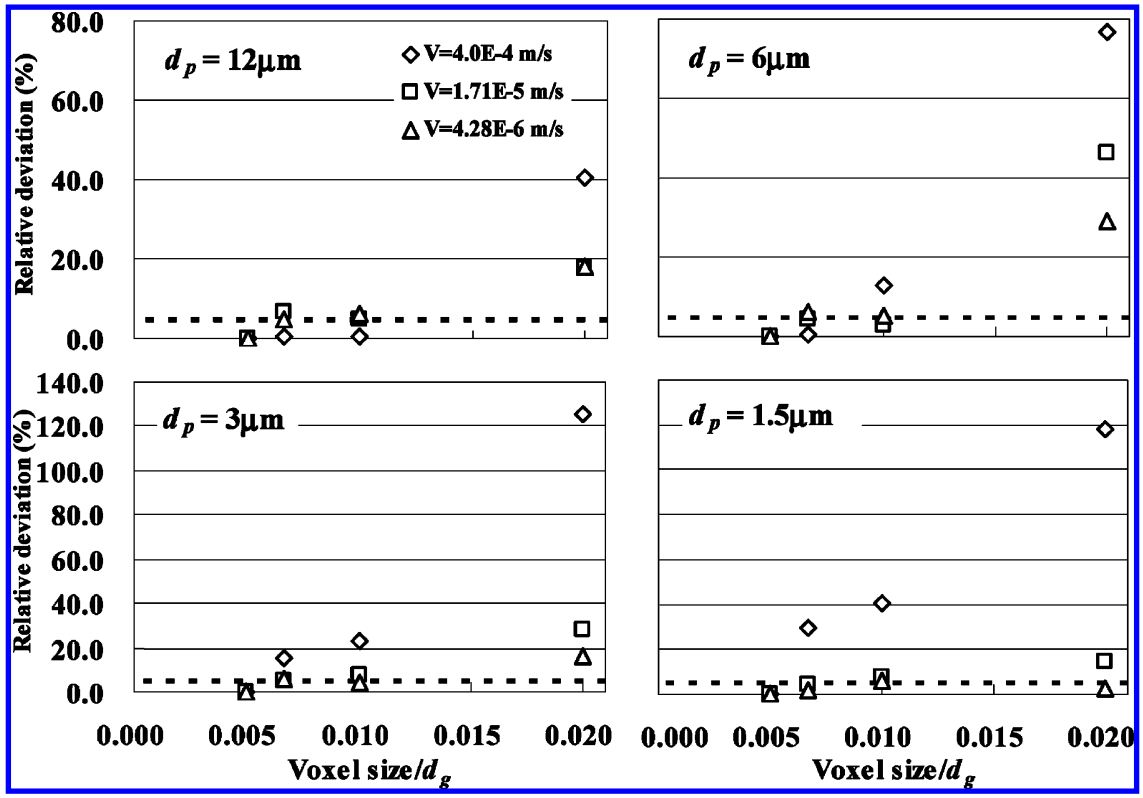

FIGURE 1. Relative deviations (%) of simulated depositions at different voxel−grain size ratios to simulated deposition at the smallest ratio (0.005) in the DC unit cell under favorable conditions (d_g = 300 μm). The relative deviations were derived by dividing the absolute value of the difference by the simulated deposition at the smallest ratio. The dashed lines represent a relative deviation of 5%.

a statistical analysis. The same set of random seeds was used for all the conditions simulated. For each run 500−30 000 particles were randomly released into the entry planes of the unit cells. The simulations were run for 480 s after each particle was released into the unit cell. The maximum simulation time (i.e., 480 s) is about 15 and 19 times the mean residence time of water molecules at the lowest superficial velocity (4.28×10^{-6} m s^{-1}) in the SC and DC unit, respectively.

During particle tracking, if a colloid reaches within 1 nm of a grain surface, attractive van der Waals interaction dominates under all conditions, and the colloid was considered deposited (attached) to the grain surface. Note that grain surface here refers to the true surface of the grain, instead of the surface in the discretized space that is not smooth. A deposited colloid was considered as deposited at grain-to-grain contacts when its separation distance to the second nearest grain was less than 100 nm. Under the flow conditions chosen for the simulation, the residence times of colloids exiting the unit cells and deposited to grain surfaces were typically within 10 and 100 s, respectively. Colloids were considered to be retained in the unit cell when its residence time reached the maximum simulation time.

Results

Sensitivity of Simulated Deposition to Discretization under Favorable Conditions. With identical colloid size, grain size, and discretization resolution, the collector efficiency in the DC unit cell (simulated number of deposited colloids divided by total number released) increased as the superficial velocity decreased, as predicted by CFT (*3, 4*) (Figure S5, Supporting Information). A significant portion but not the majority of the deposition occurred at grain-to-grain contacts (5−15%) when the colloid−grain size ratio is greater than 0.01. At smaller ratios and low fluid velocities, negligible or no deposition occurred at grain-to-grain contacts (Table S1, Supporting Information).

Simulated numbers of deposited colloids typically decreased to a significant extent as the ratio of voxel size to grain diameter decreased from 0.02 to 0.01 (Figure S5, Supporting Information). At lower ratios, simulated numbers decreased very slowly. This is especially true at the medium and low superficial velocities that represent groundwater flow regimes. In some cases, the simulated numbers at the ratios of 0.01 and 0.067 were even slightly smaller than those at the lowest ratio (Table S1, Supporting Information). Figure 1 presents the relative deviations of the total simulated numbers at higher voxel−grain size ratios (>0.005) from the simulated numbers at the lowest ratio (0.005) (grain diameter = 300 μm, colloid diameter = 1.5−12 μm). At the highest ratio (0.02), the deviation was greater than 10% and in general increased with increasing superficial velocities. The deviation was more pronounced for smaller colloid sizes at this ratio (e.g., about 125% for 3-μm colloid at a fluid velocity of 4.0×10^{-4} m s^{-1}). At the ratios equal to and less than 0.01, the deviations were all less than 10%, with an overwhelming majority less than 5% at medium and low superficial velocities. Two-tailed student *t* test indicates that at these ratios, simulated numbers are not significantly different (Table S1, Supporting Information). This is also true for submicrometer (0.5 μm) colloids. (Table S1, Supporting Information).

These findings indicate that simulated deposition under favorable conditions becomes insensitive to space discretization at a certain voxel−grain size ratio and that this critical ratio (0.01) is independent of colloid size under groundwater flow regimes. The significant difference between the deposited numbers at voxel−grain size ratios of 0.02 and 0.005 is consistent with the significant differences between the fluid velocity profiles at these two ratios (Figure 2). Likewise, the minimal difference in deposition at voxel−grain size ratios

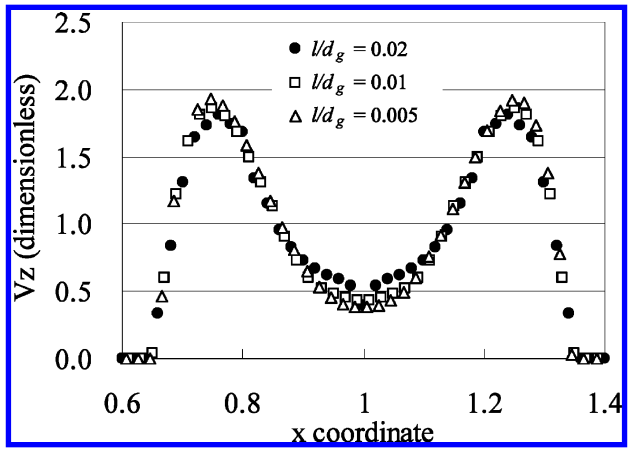

FIGURE 2. Representative fluid velocity profiles in DC unit cell at different discretization resolutions. Shown in the figure are the *z*-direction velocities (dimensionless) at the line of $y = x$ in the plane of $z = -0.914$ (the plane half of the grain radius below the entry plane). The voxel size is represented by *l*.

of 0.01 and 0.005 is consistent with the minimal difference in fluid velocity profiles at the two ratios. The velocities shown in Figure 2 are dimensionless. The absolute magnitudes of differences in the dimensional velocities (obtained by multiplying the dimensionless velocity with the superficial velocity) at the ratios of 0.02, 0.01, and 0.005 are greatest at the highest superficial velocity. This may explain why the deviations of simulated depositions at the ratios of 0.02 and 0.01 relative to 0.005 were greatest at the highest velocity (Figure 1).

Simulations using grain diameters of 150 and 600 μm revealed that the variations of simulated deposition at voxel−grain size ratio of 0.01 or below were also minimal (Table S1, Supporting Information), indicating that the same critical voxel−grain size ratio exists for grain sizes typically encountered in the subsurface. The simulated deposition decreased with increasing grain size at otherwise identical conditions (Table S1, Supporting Information), in qualitative agreement with filtration theory prediction.

In the SC unit cell, the trends of simulated deposition with respect to discretization were very similar to the trends in the DC unit cell (Figure S6, Table S2, Supporting Information). Deviations from the simulated deposition at the smallest voxel−grain size ratio were greatest at the highest fluid velocity (up to about 25%) (Figure S6, Supporting Information). However, the relative deviations were all below 7% for all colloid sizes at the medium and low velocities when the ratio is equal to or less than 0.01. This indicates that under favorable conditions the critical ratio at which simulated deposition becomes insensitive to discretization under groundwater flow conditions is independent of packing structure.

A significant number of simulated colloids remained in the SC unit cell without deposition under certain simulation conditions (Table S2, Supporting Information). The number of retained colloids seems to strongly depend on colloid sizes and fluid velocities. For example, about 85 out of 1000 simulated 6-μm colloids were retained in the system at a superficial velocity of 4.0×10^{-4} m s^{-1}, but none was retained at the two lower velocities. The cause and implication of colloid retention in SC system will be discussed in detail in the next section.

Sensitivity of Simulated Deposition to Discretization under Unfavorable Conditions. Simulations were first performed under unfavorable conditions where the energy barrier was very high (>1000 *kT*). These conditions were created by setting ionic strength at 0.001 M, colloid ζ-potential at −20 mV, and collector ζ-potential at −60 mV. Under such conditions, no deposition occurred in the SC unit cell. In the DC unit cell, deposition occurred solely at grain-to-grain contacts. Deposition decreased with decreasing superficial velocities and decreasing colloid−grain size ratios (Table S3, Supporting Information), in qualitative agreement with previous simulations using the approximate analytical solution of the flow field (*13*). For the 12-μm colloid (d_p/d_g = 0.04) at the highest velocity of 4.0×10^{-4} m s^{-1}, deposition was about 15% of the total deposition under the favorable condition with identical size and velocity (Tables S1 and S3, Supporting Information). Deposition at grain-to-grain contacts decreased to zero for colloids smaller than 6 μm at the highest velocity and for all colloid sizes at the medium and low superficial velocities.

In order to examine the sensitivity of deposition to space discretization under groundwater flow regimes, the energy barrier was lowered to a few *kT*. Under such conditions, diffusion allowed a significant amount of colloids to overcome the energy barrier (Table S3, Supporting Information). For the 3-μm colloid, at a solution ionic strength of 0.006 M and a collector ζ-potential of −12 mV, the energy barrier increased from 1.1 to 6.8 *kT*, as the colloid ζ-potential decreased from −3.7 to −4.2 mV. The secondary minimum depths at the two conditions were 2.8 and 2.6 *kT*, respectively. Total deposition decreased from 88 out of 1500 simulated colloids to 15 out of 5000 simulated colloids, at a fluid velocity of 1.71×10^{-5} m s^{-1} and a collector diameter of 300 μm (simulated at a voxel−grain size ratio of 0.005). The deposition under the two conditions translated to collision efficiencies (ratios of deposition under unfavorable conditions to deposition under favorable conditions) of 0.72 and 0.037, respectively. That simulated collision efficiencies decrease with increasing energy barriers is consistent with expectation.

Under the low-energy barrier conditions examined, deviations of simulated total deposition were also around or less than 5% at the voxel−grain size ratio of 0.01 for colloids with diameters down to 1.0 μm (d_g = 300 μm) at the medium and lower fluid velocities in both packing systems (Figure 3, Tables S3 and S4, Supporting Information). This is also true at both fluid velocities for the collector of 150 μm and at the lower fluid velocity for the collector of 600 μm. In contrast, simulated deposition of the 0.5-μm colloid at the voxel−grain size ratio of 0.01 deviated from deposition at the lowest ratio by more than 10% even at the lowest fluid velocity (Figure 3, Tables S3 and S4, Supporting Information). It is worth noting that under unfavorable conditions, simulated deposition increased with decreasing voxel−grain size ratios for smaller colloids (Tables S3 and S4, Supporting Information), whereas an opposite trend was observed under favorable conditions (Tables S1 and S2, Supporting Information). This difference is explained in the next section.

Discussion

Sensitivity of Simulated Flow Fields Near Grain Surface to Discretization. In the discretized space, the grain surface is no longer smooth. As a result, the errors of the simulated fluid velocities are expected to be greatest near the grain surface. The errors of near surface velocities would have greater impacts on simulated deposition of smaller colloids, as the centers of larger colloids would not get into the closest distances of grain surfaces (i.e., near surface velocities are not involved in simulations of large colloids). To examine how these errors affect the simulated deposition, the average *z*-direction fluid velocities near grain surfaces were extracted from the simulated flow field using the approach described in the Supporting Information.

At a distance of 3 μm or above, the simulated average velocity increases with decreasing voxel−grain size ratio at a grain diameter of 300 μm. The trend was reversed for simulated average velocities at closer distances (Figure S7,

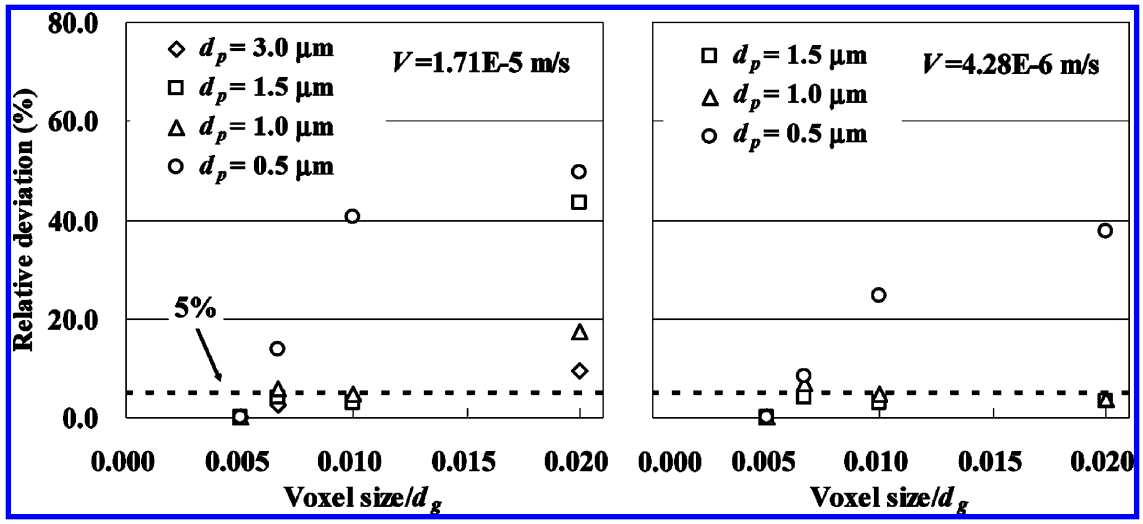

FIGURE 3. Relative deviations (%) of simulated depositions at different voxel−grain size ratios to simulated deposition at the smallest ratio (0.005) in the DC unit cell under unfavorable conditions (d_g = 300 μm).

left, Supporting Information). The magnitude of the simulated average *z*-direction fluid velocity decreases considerably from 2.35 (dimensionless here) at a distance of 6 μm to 0.17 at a distance of 0.25 μm. As such, the relative deviation of the simulated fluid velocity at a particular voxel−grain size ratio from the simulated velocity at the lowest ratio is much greater at closer distances (Figure S7, right, Supporting Information).

Under favorable conditions, deposition is largely affected by mass transport to the grain surface, as all the colloids colliding with the grain surface would deposit. Therefore. the flow field away from the grain surface plays a more important role in colloid deposition as this portion of the flow field determines the mass transport. According to the filtration theory, greater mass transport (represented by the single collector efficiency) occurs at lower superficial velocity (*3, 4*). Hence, decreasing simulated velocities away from surface with decreasing voxel−grain size ratios is consistent with the greater simulated deposition at larger ratios (Tables S1 and S2, Supporting Information).

Under unfavorable conditions, colloid deposition is affected not only by the mass transport to the grain surface but also by the diffusion (over the energy barrier) at the proximity of the surface. At lower near surface fluid velocities, colloids transported to grain surfaces stay close to the surfaces for longer time. As a result, more colloids would diffuse over the barrier to deposit. Therefore, under unfavorable conditions, simulated colloid deposition is subject to the interplay of the increasing simulated fluid velocities at closer distances with increasing voxel−grain size ratios and the opposite trend at greater distances. The least simulated deposition of most colloid sizes at the greatest voxel−grain size ratio of 0.02 (Tables S3 and S4, Supporting Information) may well be due to the fact that the former trend dominated the interplay. The significant deviation of simulated deposition of the 0.5-μm colloids at a voxel−grain size ratio of 0.01 (Tables S3 and S4, Supporting Information) may also be due to the dominance of the former trend. A balance of the two trends may explain the minimal deviation of simulated deposition at a voxel−grain size ratio of 0.01 for colloids down to 1 μm.

Estimation of Simulation Times for Assemblage-Scale Porous Medium Domains. The finding that simulated deposition tends to become asymptotic at a critical voxel−grain size ratio of 0.01 for colloids with sizes down to submicrometer levels under favorable conditions and down to around 1 μm under unfavorable conditions has enormous implications for colloid transport simulations. First, it greatly simplifies the strategies to discretize pore spaces for flow field simulations in porous media typically encountered in laboratories and fields. For example, a fixed discretization resolution (voxel size equal to 1% of the average grain diameter) can be used for all conditions for well-sorted porous media. For poorly sorted porous media, the voxel size can be conservatively set at $^1/_{100}$ of the smallest grains.

Second, this finding indicates that tracking transport of colloids with size down to around 1 μm (i.e., size of bacteria) in an assemblage domain of porous media consisting of spherical collectors (e.g., glass beads) is computationally feasible. The glass beads can be approximated as spheres whose centers (and surfaces) can be identified from reconstructed XMT images (e.g., refs *10, 11*). The limiting factor of particle tracking in assemblage domains would be the LB simulations of the flow fields because computation of particle tracking increases arithmetically with domain size, whereas computation of a flow field increases exponentially (at a power of about 4 of the size). A flow simulation of a domain of 200 × 200 × 200 voxels at a typical porosity of 0.36 takes about 3 days on a personal computer (with a RAM of 2 gigabytes). For an assemblage domain that consists of 10 grains in each dimension, about 1000 lattices in each dimension are needed (assuming a voxel−grain size ratio of 0.01). This would take about 1900 (=3×5^4) days on a personal computer, which is prohibitively too long. Nevertheless, given the easy parallelization of LB simulations, it is reasonably expected that simulations run simultaneously on a few hundred processors that are available at typical computation centers would reduce the computational time down to a few days. This is, of course, still very expensive but is acceptable, as only one simulation is required to obtain the dimensionless flow field and this flow field can be used for particle tracking at different superficial velocities (as was done in this work). Simulations at assemblage-scale domains can not only validate LB method-based particle tracking by comparing simulated collector efficiencies to experimentally determined values but also examine mechanistically various deposition processes (e.g., retention in zones of flow stagnation).

Retention of Colloids in Flow Vortices. Retention of colloid in SC unit cell without deposition was also reported in the previous simulations that used the approximate analytical solution of the flow field (*13*). A number of differences, however, exist between the findings of this and the previous work. First, only small colloids (≤3 μm) were retained at low superficial velocities (≤1.71×10^{-5} m s^{-1}), whereas in this work colloids with sizes up to 6 μm were retained at the highest velocity. Second, colloid retention

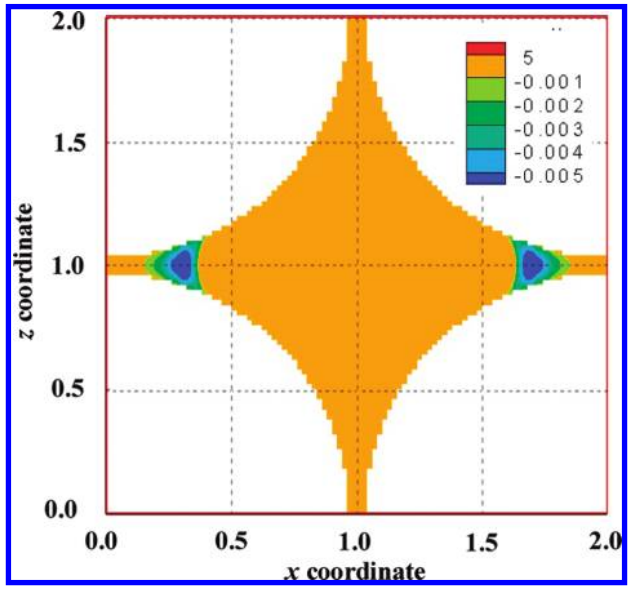

FIGURE 4. Representative 2-D flow field (in the plane of $y = 0.28$) showing the flow vortices (regions where fluid velocities are negative) in the SC unit cell. White areas are grains. Yellow color represents fluid velocities in the range of 0−5. The unit cell was discretized at a voxel−grain size ratio of 0.01.

was found to occur only under unfavorable conditions, whereas this work shows that it could occur under both favorable and unfavorable conditions. Most importantly, previous work demonstrated that retained colloids (with small sizes and mainly in the SC unit cell) are associated with the secondary energy minimum (a few to a few tens of nanometers from the grain surface), whereas this work indicates that separation distances between retained colloids and the closest grain surface can be over 10 μm (Figure S8, Supporting Information). The retained colloids in this work are confined in certain regions, as the normalized x-, y-, and z-coordinates of the retained colloids vary by no more than 0.12 (translating into about 18-μm at a grain radius of 150 μm) (Figure S8, Supporting Information). In particular, its z-coordinate appears to oscillate around the entry plane ($z = 1$). Note that when the z-coordinate of the colloid is less than 1, it is assigned with the velocity at $z + 2$ according to the periodicity of the unit cell (keeping x- and y-coordinates constant). Note also that particle tracking of small colloids (with diameter less than 0.5 μm) in SC unit cell would take much longer simulation time and so was not performed in this work. Future work is needed to parallelize the particle tracking code here to examine whether simulations using discrete flow fields would also demonstrate retention via association with the secondary minimum.

That colloids can leave the unit cell from the entry plane for significant distances indicates that the colloids must be experiencing flow that is in the opposite direction of the overall flow. This can occur only when there are flow vortices in the system. Plotting the flow field indeed shows flow vortices that are located close to the contact areas between the grains (Figure 4). The magnitude of the maximum velocity in the vortices is about 0.6% of the superficial velocity (in opposite direction however). Examination of initial positions of retained colloids reveals that retained colloids were released directly into or very close to the flow vortices (Figure S9, Supporting Information). Flow vortices near grain contact areas have been previously demonstrated by Biggs et al. and recently by Cardenas and Torkzaban et al. (*22*−*24*). Boutt et al. found that flow vortices (they called it recirculation zones) also existed in a single fracture (*25*). Furthermore, Biggs et al. and Boutt et al. demonstrated that colloids could be retained or trapped in the flow vortices (*22, 25*). Particle tracking in this work provides an additional mechanistic conformation of this retention process.

Because electric double layer and van der Waals forces are negligible at large separation distance, colloids in vortices mainly experiences random Brownian motion, downward gravity, and upward fluid drag force emanating from the vortices (overall flow downward). The interplay of these three forces may explain the trends of simulated number of retained colloids. At the highest superficial velocity and under favorable conditions, the number of retained colloids increased from about 30 (out of 1000 colloids simulated) for the 1.5-μm colloid, to about 60 for the 3-μm colloid, further to about 85 for the 6-μm colloid, and decreased to 0 for the 12-μm colloid (Table S2, Supporting Information). Zero retention of the 12-μm colloid could well be caused by domination of its gravity, whereas decreasing retention with decreasing colloid sizes may be due to increasing Brownian motion that drives the colloids out of the vortices.

Retention in flow vortices shown here has important implications. Under conditions extremely unfavorable for deposition (e.g., very low ionic strength or very high pH), interaction energy calculations would show that the energy barrier is too high to allow deposition and the secondary energy minimum too shallow to hold colloids from diffusion (*26*). Retention in flow vortices largely as a pure physical process may explains observed colloid removal by porous media under such conditions. Diffusion of retained colloids out of flow vortices may also explain the persistent low colloid concentrations following breakthrough (extended tailing) that have been observed both in laboratory and field studies (e.g., refs *27, 28)*. In fact, recent simulations by Cardenas indicated that vortices could be a source of tailing behavior in solute transport in simple cubic packing system (*23*). Further investigation is needed to examine whether flow vortices are widely present in real porous media and to determine whether and how much colloids can get into and diffuse out of flow vortices under different solution chemistry and flow conditions.

Acknowledgments

This work is funded by the National Science Foundation of China (Grant No. 40772147). The authors wish to thank Prof. William P. Johnson and Dr. Huilan Ma at the Department of Geology and Geophysics of the University of Utah for providing the particle tracking code and for their helpful inputs during the development of the manuscript.

Supporting Information Available

LB flow simulations, fluid velocity interpolation schemes, modification of the particle tracking algorithm, extraction of average near-surface fluid velocities, trajectories and initial positions of retained colloids in the unit cell of the simple packing system, and tabulated results of simulations. This material is available free of charge via the Internet at http://pubs.acs.org.

Literature Cited

(1) Yao, K. M.; Habibian, M. T.; O'Melia, C. R. Water and waste water filtration: Concepts and applications. *Environ. Sci. Technol.* **1971**, *5* (11), 1105–1112.
(2) Happel, J. Viscous flow in multiparticle systems: Slow motion of fluids relative to beds of spherical particles. *AIChE J.* **1958**, *4* (2), 197–201.
(3) Tufenkji, N.; Elimelech, M. Correlation equation for predicting single-collector efficiency in physicochemical filtration in saturated porous media. *Environ. Sci. Technol.* **2004**, *38*, 529–536.
(4) Rajagopalan, R.; Tien, C. Trajectory analysis of deep-bed filtration with the sphere-in-cell porous media model. *AIChE J.* **1976**, *22* (3), 523–533.
(5) Nelson, K. E.; Ginn, T. R. Colloid filtration theory and the Happel sphere-in-cell model revisited with direct numerical simulation of colloids. *Langmuir* **2005**, *21* (6), 2173–2184.

(6) Li, X.; Scheibe, T. D.; Johnson, W. P. Apparent decreases in colloid deposition rate coefficient with distance of transport under unfavorable deposition conditions: A general phenomenon. *Environ. Sci. Technol.* **2004**, *38* (21), 5616–5625.
(7) Elimelech, M.; O'Melia, C. R. Kinetics of deposition of colloidal particles in porous media. *Environ. Sci. Technol.* **1990**, *24* (10), 1528–1536.
(8) Bhattacharjee, S.; Ko, C. H.; Elimelech, M. DLVO interaction between rough surfaces. *Langmuir* **1998**, *14*, 3365–3375.
(9) Shellenberger, K.; Logan, B. E. Effect of molecular scale roughness of glass beads on colloidal and bacterial deposition. *Environ. Sci. Technol.* **2002**, *36* (2), 184–189.
(10) Li, X.; Lin, C. L.; Miller, J.; Johnson, W. P. Pore-scale observation of microsphere deposition at grain-grain contacts over assemblage-scale porous media using X-ray microtomography. *Environ. Sci. Technol.* **2006**, *40*, 3762–3768.
(11) Li, X.; Lin, C. L.; Miller, J.; Johnson, W. P. Role of grain to grain contacts on profiles of retained colloids in porous media in the presence of an energy barrier to deposition. *Environ. Sci. Technol.* **2006**, *40*, 3769–3774.
(12) Cushing, R. S.; Lawler, D. F. Depth filtration: Fundamental investigation through three-dimensional trajectory. *Environ. Sci. Technol.* **1998**, *32*, 3793–3801.
(13) Johnson, W. P.; Li, X.; Yal, G. Colloid retention in porous media: Mechanistic confirmation of wedging and retention in zones of flow stagnation. *Environ. Sci. Technol.* **2007**, 1279–1287.
(14) Johnson, W. P.; Tong, M.; Li, X. On colloid retention in saturated porous media in the presence of energy barriers: The failure of α, and opportunities to predict η. *Water Resour. Res.* **2007**, *43*, W12S13, (doi: 10.1029/2006WR005770).
(15) Lin, C. L.; Miller, J. D. Pore structure analysis of particle beds for fluid transport simulation during filtration. *Int. J. Miner. Process.* **2004**, *73*, 281–294.
(16) Chen, S.; Doolen, G. D. Lattice Boltzmann method for fluid flows. *Annu. Rev. Fluid Mech.* **1998**, *30*, 329–364.
(17) Chen, C.; Packman, A. I.; Gaillard, J. F. Pore-scale analysis of permeability reduction resulting from colloid deposition. *Geophys. Res. Lett.* **2008**, *35*, L07404, (doi: 10.1029/2007GL033077).
(18) Chen, C.; Lau, B. L. T.; Gaillard, J. F.; Packman, A. I. Temporal evolution of pore geometry, fluid flow, and solute transport resulting from colloid deposition. *Water Resour. Res.* **2009**, *43*, W06416, (doi: 10.1029/2008WR007252).
(19) Creber, S. A.; Pintelon, T. R. R.; Johns, M. L. Quantification of the velocity acceleration factor for colloidal transport in porous media using NMR. *J. Colloid Interface Sci.* **2009**, *339*, 168–174.
(20) Maier, R. B.; Bernard, R. S.; Grunau, D. W. Boundary conditions for the lattice Boltzmann method. *Phys. Fluids* **1996**, *8* (7), 1788–1801.
(21) Zou, Q.; He, X. On pressure and velocity boundary conditions for the lattice Boltzmann BGK model. *Phys. Fluids* **1997**, *9* (6), 1591–1598.
(22) Biggs, M. J.; Humby, S. J.; Buts, A.; Tüzün, U. Explicit numerical simulation of suspension flow with deposition in porous media: Influence of local flow field variation on deposition processes predicted by trajectory methods. *Chem. Eng. Sci.* **2003**, *58*, 1271–1288.
(23) Cardenas, M. B. Three-dimensional vortices in single pores and their effects on transport. *Geophys. Res. Lett.* **2008**, *35*, L18402, (doi: 10.1029/2008GL035343).
(24) Torkzaban, S.; Tazehkand, S. S.; Walker, S. L.; Bradford, S. A. Transport and fate of bacteria in porous media: Coupled effects of chemical conditions and pore space geometry. *Water Resour. Res.* **2008**, *44*, W04403, (doi: 10.1029/2007WR006541).
(25) Boutt, D. F.; Grasselli, G.; Fredrich, J. T.; Cook, B. K.; Williams, J. R. The effect of fracture roughness on the directional anisotropy of fluid flow and colloid transport in a single fracture. *Geophys. Res. Lett.* **2006**, *33*, L21402, (doi: 10.1029/2006GL027275).
(26) Hahn, M. W.; O'Melia, C. R. Deposition and reentrainment of Brownian particles in porous media under unfavorable chemical conditions: Some concepts and applications. *Environ. Sci. Technol.* **2004**, *38*, 210–220.
(27) Li, X.; Zhang, P.; Lin, C. L.; Johnson, W. P. Role of hydrodynamic drag on microsphere deposition and re-entrainment in porous media under unfavorable deposition conditions. *Environ. Sci. Technol.* **2005**, *39* (11), 4012–4020.
(28) Zhang, P.; Johnson, W. P.; Scheibe, T. D.; Choi, K.; Dobbs, F. C.; Mailloux, B. J. Extended tailing of bacteria following breakthrough at the Narrow Channel Focus Area, Oyster, Virginia. *Water Resour. Res.* **2001**, *37* (11), 2687–2698.

ES9027716